

Parton coalescence at RHIC

V. Greco and C. M. Ko

Cyclotron Institute and Physics Department, Texas A&M University, College Station, Texas 77843-3366, USA

P. Lévai

KFKI Research Institute for Particle and Nuclear Physics, P.O. Box 49, Budapest 1525, Hungary

(Dated: February 8, 2008)

Using a covariant coalescence model, we study hadron production in relativistic heavy ion collisions from both soft partons in the quark-gluon plasma and hard partons in minijets. Including transverse flow of soft partons and independent fragmentation of minijet partons, the model is able to describe available experimental data on pion, kaon, and antiproton spectra. The resulting antiproton to pion ratio is seen to increase at low transverse momenta and reaches a value of about one at intermediate transverse momenta, as observed in experimental data at RHIC. A similar dependence of the antikaon to pion ratio on transverse momentum is obtained, but it reaches a smaller value at intermediate transverse momenta. At high transverse momenta, the model predicts that both the antiproton to pion and the antikaon to pion ratio decrease and approach those given by the perturbative QCD. Both collective flow effect and coalescence of minijet partons with partons in the quark-gluon plasma affect significantly the spectra of hadrons with intermediate transverse momenta. Elliptic flows of protons, Lambdas, and Omegas have also been evaluated from partons with elliptic flows extracted from fitting measured pion and kaon elliptic flows, and they are found to be consistent with available experimental data.

PACS numbers: 25.75.-q, 25.75.Dw, 25.75.Nq, 12.38.Bx

I. INTRODUCTION

Recently, there is a renewed interest in using the parton coalescence or recombination model to understand hadron production from the quark-gluon plasma formed in relativistic heavy ion collisions [1, 2, 3, 4, 5, 6]. Emphases in these studies are, however, different from earlier ones based on the coalescence model such as the ALCOR [7] and the MICOR [8] model. Instead of addressing particle yields and their ratios, these new studies were more concerned with observables related to collective dynamics and production of hadrons with relatively large transverse momentum. In Ref. [1], the parton coalescence was used to convert the quark matter, that is formed from melted soft strings produced in initial soft collisions, to hadrons. Including parton coalescence in a multiphase transport model (AMPT) [9], it was found that partonic effects are important for describing measured large elliptic flows and narrow two-pion correlation functions at RHIC. In Ref. [2], it was shown that hadron production based on parton coalescence is able to account for the qualitative difference between the observed elliptic flows of mesons and baryons. Based on parton recombination, a parton transverse momentum distribution is obtained in Ref. [3] from the measured pion spectrum and is then used to predict the kaon and proton transverse momentum spectra. The parton coalescence model is further found in Refs. [4, 5] to be able to explain the observed enhancement of intermediate transverse momentum protons and antiproton. While coalescence of partons from a quark-gluon plasma with high effective temperature is considered in Ref. [4], their coalescence with minijet partons is introduced in Ref. [5] as a new mechanism for

hadronization of minijet partons.

Besides independent fragmentations to hadrons as usually considered, minijet partons produced in relativistic heavy ion collisions [10] are allowed in Ref. [5] to coalesce with partons from the quark-gluon plasma formed in relativistic heavy ion collisions, as suggested in Ref. [6] for studying the flavor ordering of the elliptic flows of hadrons with intermediate transverse momenta. Since minijet partons have a power-law transverse momentum spectrum while partons in the quark-gluon plasma have an exponential thermal spectrum, this mechanism leads to an enhanced production of hadrons with intermediate transverse momentum. Because of stronger enhancement for baryons and antibaryons than for pions from this hadronization mechanism, a large antiproton to pion ratio of about one is obtained at intermediate transverse momenta as seen in the experimental data from the PHENIX collaboration [11]. However, in this study hadrons from hadronization of the quark-gluon plasma are taken to also have exponential thermal spectra extending to all transverse momenta. Furthermore, in order to obtain a semi-analytical expression for the coalescence formula, only comoving partons at zero rapidity are considered in evaluating the coalescence probability for hadron production. Although relativistic kinematics was used in this study, the model is not fully covariant. In the present paper, we relax these simplifications by using a covariant coalescence model and treating more generally parton coalescence via a Monte-Carlo method. Also, we include coalescence among partons from the quark-gluon plasma so that hadrons with low momenta are treated on the same footing as those with intermediate momenta. We show that this improved coalescence model for par-

tons from both the quark-gluon plasma and minijets is able to reproduce the experimental transverse momentum spectra of pions, antikaons, and antiprotons measured at RHIC as well as the antiproton to pion ratio as functions of transverse momentum. We further predict the dependence of the K^-/π^- ratio on transverse momentum. Fitting quark elliptic flows to measured pion and kaon elliptic flows, the predicted elliptic flows of protons and Λ are found to agree with available experimental data. The Ω elliptic flow is also predicted and is smaller than that of Λ as a result of smaller elliptic flow for light quarks than strange quarks.

The paper is organized as follows. In Section II, we describe the general formalism of a covariant coalescence model for mesons and baryons. How minijet and quark-gluon plasma partons are determined for Au+Au collisions at 200 AGeV are described in Section III. In Section IV, the Monte-Carlo method used for treating coalescence among partons whose numbers vary by many orders of magnitude is presented. Results for the transverse momentum spectra of pions, antiprotons, and antikaons obtained from the coalescence model are given in Section V. Ratios of the antiproton to pion and the antikaon to pion transverse momentum spectra are also shown. We further study the effect of coalescence of minijet partons with those in the quark-gluon plasma and also the effect of collective flow on the spectra and ratios of produced hadrons. The elliptic flow of hadrons based on that of quarks is also studied. Finally, we conclude in Section VIII with a summary of present work and an outlook about future developments and applications of the parton coalescence model.

II. THE COALESCENCE MODEL

Using the covariant coalescence model of Dover *et al.* [12], the number of mesons formed from the coalescence of quark and antiquarks can be written as

$$N_M = g_M \int p_1 \cdot d\sigma_1 p_2 \cdot d\sigma_2 \frac{d^3 \mathbf{p}_1}{(2\pi)^3 E_1} \frac{d^3 \mathbf{p}_2}{(2\pi)^3 E_2} \times f_q(x_1; p_1) f_{\bar{q}}(x_2; p_2) f_M(x_1, x_2; p_1, p_2). \quad (1)$$

In the above, $d\sigma$ denotes an element of a space-like hypersurface; and g_M is the statistical factor for forming a colorless meson from spin 1/2 color quark and antiquark. For mesons considered here, i.e., π , ρ , K , and K^* , the statistical factors are $g_\pi = g_K = 1/36$ and $g_\rho = g_{K^*} = 1/12$. The functions $f_q(x, p)$ and $f_{\bar{q}}(x, p)$ are, respectively, covariant distribution functions of quarks and antiquarks in the phase space, and they are normalized to their numbers, i.e.,

$$\int p \cdot d\sigma \frac{d^3 \mathbf{p}}{(2\pi)^3 E} f_{q,\bar{q}}(x, p) = N_{q,\bar{q}}. \quad (2)$$

The function $f_M(x_1, x_2; p_1, p_2)$ in Eq.(1) is the probability for a quark and an antiquark to form a meson. It

describes the dynamic process of converting a quark and an antiquark to a bound state meson in the presence of a partonic matter. It depends on the overlap of the quark and antiquark wave functions with the wave function of the meson as well as the interactions of emitted virtual partons, which are needed for balancing the energy and momentum, with the partonic matter. Neglecting the off-shell effects and taking the wave functions of quark and antiquark to be plane waves, the coalescence probability function is then simply the covariant meson Wigner distribution function. In Ref. [12], it is parametrized by Gaussian functions in $x_1 - x_2$ and $p_1 - p_2$. Here, we take it to have a uniform distribution as in Ref. [5], i.e.,

$$f_M(x_1, x_2; p_1, p_2) = \frac{9\pi}{2(\Delta_x \Delta_p)^3} \Theta(\Delta_x^2 - (x_1 - x_2)^2) \times \Theta(\Delta_p^2 - (p_1 - p_2)^2 + (m_1 - m_2)^2), \quad (3)$$

where Δ_x and Δ_p are the covariant spatial and momentum coalescence radii. The factors in front of theta functions are introduced to obtain the correct normalization for the meson Wigner function in the nonrelativistic limit. Here we use $\hbar = c = 1$.

For ultrarelativistic heavy ion collisions at RHIC, it is convenient to introduce rapidities variables y and η in the momentum and the coordinate space, respectively, and they are defined by

$$y = \frac{1}{2} \ln \frac{E + p_z}{E - p_z}, \quad \eta = \frac{1}{2} \ln \frac{t + z}{t - z}. \quad (4)$$

Using these variables, the spatial coordinate becomes $x = (\tau \cosh \eta, -\tau \sinh \eta, -\mathbf{r}_T)$, with $\tau = \sqrt{t^2 - z^2}$ and \mathbf{r}_T denoting, respectively, proper time and transverse coordinates; while the momentum is $p = (m_T \cosh y, -m_T \sinh y, -\mathbf{p}_T)$ with $m_T = \sqrt{m_q^2 + \mathbf{p}_T^2}$ being the transverse mass in terms of quark mass m_q and its transverse momentum \mathbf{p}_T . The momentum volume element is then given by

$$\frac{d^3 \mathbf{p}}{E} = dy d^2 \mathbf{p}_T, \quad (5)$$

while the spatial volume element becomes

$$p \cdot d\sigma = \tau m_T \cosh(y - \eta) d\eta d^2 \mathbf{r}_T, \quad (6)$$

if we adopt a hypersurface of constant longitudinal proper times.

The quark and antiquark phase space distribution functions are then given by

$$f_{q,\bar{q}}(x, p) = \frac{(2\pi)^3}{\tau m_T \cosh(y - \eta)} \frac{dN_{q,\bar{q}}}{d\eta d^2 \mathbf{r}_T dy d^2 \mathbf{p}_T}, \quad (7)$$

where R_\perp is the transverse radius of the system.

The yield of mesons from coalescence of quarks and

antiquarks is then given by

$$\begin{aligned}
N_M &= g_M \int d\eta_1 d^2\mathbf{r}_{1T} d\eta_2 d^2\mathbf{r}_{2T} dy_1 d^2\mathbf{p}_{1T} dy_2 d^2\mathbf{p}_{2T} \\
&\times \frac{dN_q}{d\eta_1 d^2\mathbf{r}_{1T} dy_1 d^2\mathbf{p}_{1T}} \frac{dN_{\bar{q}}}{d\eta_2 d^2\mathbf{r}_{2T} dy_2 d^2\mathbf{p}_{2T}} \\
&\times f_M(x_1, x_2; p_1, p_2). \quad (8)
\end{aligned}$$

The transverse momentum spectrum of mesons can be obtained from Eq.(12) by multiplying the right hand side with

$$1 = \int d^2\mathbf{p}_T \delta^{(2)}(\mathbf{p}_T - \mathbf{p}_{1T} - \mathbf{p}_{2T}), \quad (9)$$

and then differentiating both sides of the equation with respect to \mathbf{p}_T . The resulting meson transverse momentum spectrum from quark and antiquark coalescence is given by

$$\begin{aligned}
\frac{dN_M}{d^2\mathbf{p}_T} &= g_M \int d\eta_1 d^2\mathbf{r}_{1T} d\eta_2 d^2\mathbf{r}_{2T} dy_1 d^2\mathbf{p}_{1T} \\
&\times dy_2 d^2\mathbf{p}_{2T} \frac{dN_q}{d\eta_1 d^2\mathbf{r}_{1T} dy_1 d^2\mathbf{p}_{1T}} \frac{dN_{\bar{q}}}{d\eta_2 d^2\mathbf{r}_{2T} dy_2 d^2\mathbf{p}_{2T}} \\
&\times f_M(x_1, x_2; p_1, p_2) \delta^{(2)}(\mathbf{p}_T - \mathbf{p}_{1T} - \mathbf{p}_{2T}). \quad (10)
\end{aligned}$$

For quarks and antiquarks produced at central rapidities in relativistic heavy ion collisions, it is reasonable to assume that their longitudinal momentum distributions are boost-invariant, i.e., independent of rapidity. Furthermore, they are expected to satisfy the Bjorken correlation of equal spatial and momentum rapidities, i.e., $\eta = y$. The quark and antiquark phase space distribution functions in the rapidity range Δy can then be expressed as

$$\frac{dN_{q,\bar{q}}}{d\eta d^2\mathbf{r}_T dy d^2\mathbf{p}_T} = \frac{\delta(\eta - y)}{\Delta y} \frac{dN_{q,\bar{q}}}{d^2\mathbf{r}_T d^2\mathbf{p}_T} \Big|_{|y| \leq \Delta y/2}. \quad (11)$$

This leads to the following meson transverse momentum spectrum from coalescence of quarks and antiquarks

$$\begin{aligned}
\frac{dN_M}{d^2\mathbf{p}_T} &= \frac{g_M}{(\Delta y)^2} \int d^2\mathbf{r}_{1T} d^2\mathbf{r}_{2T} d^2\mathbf{p}_{1T} d^2\mathbf{p}_{2T} \\
&\times \frac{dN_q}{d^2\mathbf{r}_{1T} d^2\mathbf{p}_{1T}} \Big|_{|y_1| \leq \Delta y/2} \frac{dN_{\bar{q}}}{d^2\mathbf{r}_{2T} d^2\mathbf{p}_{2T}} \Big|_{|y_2| \leq \Delta y/2} \\
&\times \int d\eta_1 dy_1 d\eta_2 dy_2 \delta(\eta_1 - y_1) \delta(\eta_2 - y_2) \\
&\times f_M(x_1, x_2; p_1, p_2) \delta^{(2)}(\mathbf{p}_T - \mathbf{p}_{1T} - \mathbf{p}_{2T}). \quad (12)
\end{aligned}$$

The above result can be simplified if there is no correlation between parton transverse momenta and positions, such as in the absence of collective transverse flow, and if partons are also uniformly distributed in the transverse space. In this case, the quark and antiquark distributions only depend on transverse momentum, i.e.,

$$\frac{dN_{q,\bar{q}}}{d^2\mathbf{r}_T d^2\mathbf{p}_T} \Big|_{|y| \leq \Delta y/2} = \frac{1}{\pi R_{\perp}^2} \frac{dN_{q,\bar{q}}}{d^2\mathbf{p}_T} \Big|_{|y| \leq \Delta y/2}. \quad (13)$$

Considering small rapidity range such as $\Delta y \leq 1$, we have

$$\begin{aligned}
(x_1 - x_2)^2 &= 2\tau^2 [1 - \cosh(\eta_1 - \eta_2)] - (\mathbf{r}_{1T} - \mathbf{r}_{2T})^2 \\
&\approx -\tau^2 (\eta_1 - \eta_2)^2 - (\mathbf{r}_{1T} - \mathbf{r}_{2T})^2 \\
&\approx -(\mathbf{r}_1 - \mathbf{r}_2)^2, \quad (14)
\end{aligned}$$

and

$$\begin{aligned}
(p_1 - p_2)^2 &= m_{1T}^2 + m_{2T}^2 - 2m_{1T}m_{2T} \cosh(y_1 - y_2) \\
&\quad - (\mathbf{p}_{1T} - \mathbf{p}_{2T})^2 \\
&\approx (m_{1T} - m_{2T})^2 - (\mathbf{p}_{1T} - \mathbf{p}_{2T})^2. \quad (15)
\end{aligned}$$

After carrying out the integrals in transverse space, the meson transverse momentum spectra is then give by

$$\begin{aligned}
\frac{dN_M}{d^2\mathbf{p}_T} &= g_M \frac{6\pi}{\tau \Delta y R_{\perp}^2 \Delta_p^3} \int d^2\mathbf{p}_{1T} d^2\mathbf{p}_{2T} \\
&\times \frac{dN_q}{d^2\mathbf{p}_{1T}} \Big|_{|y_1| \leq \Delta y/2} \frac{dN_{\bar{q}}}{d^2\mathbf{p}_{2T}} \Big|_{|y_2| \leq \Delta y/2} \\
&\times \delta^{(2)}(\mathbf{p}_T - \mathbf{p}_{1T} - \mathbf{p}_{2T}) \Theta(\Delta_p^2 - (\mathbf{p}_{1T} - \mathbf{p}_{2T})^2) \\
&\quad - [(m_{1T} - m_{2T})^2 - (m_1 - m_2)^2]. \quad (16)
\end{aligned}$$

This result for meson transverse momentum spectra reduces to that used in our previous schematic study [5] if we assume that only comoving quarks and antiquarks can coalesce to hadrons and replace the arguments of theta functions in Eq.(16) by Δ_p^2 minus quark and antiquark relative momentum in meson rest frame.

Since we will include collective transverse flow of partons in the quark-gluon plasma, Eq.(12) will be used in the following study. To generalize the results for mesons to formation of baryons and antibaryons from the parton distribution functions, we take the baryon coalescence probability function as

$$\begin{aligned}
F_B(x_1, x_2, x_3; p_1, p_2, p_3) &= \frac{9\pi}{2\Delta_x^3 \Delta_p^3} \Theta\left(\Delta_x^2 - \frac{1}{2}(x_1 - x_2)^2\right) \\
&\times \Theta\left(\Delta_p^2 - \frac{1}{2}(p_1 - p_2)^2\right) \\
&\times \frac{9\pi}{2\Delta_x^3 \Delta_p^3} \Theta\left(\Delta_x^2 - \frac{1}{6}(x_1 + x_2 - 2x_3)^2\right) \\
&\times \Theta\left(\Delta_p^2 - \frac{1}{6}[(p_1 + p_2 - 2p_3)^2 - (m_1 + m_2 - 2m_3)^2]\right), \quad (17)
\end{aligned}$$

where we have taken for simplicity the same space and momentum coalescence radii for the relative Jacobi coordinates among three quarks.

For boost-invariant dynamics with Bjorken spatial and momentum rapidities correlation, we obtain following baryon transverse momentum spectrum from coalescence

of three quarks:

$$\begin{aligned} \frac{dN_B}{d^2\mathbf{p}_T} &= \frac{g_B}{(\Delta y)^3} \int \prod_{i=1}^3 d^2\mathbf{r}_{iT} d^2\mathbf{p}_{iT} \frac{dN_q}{d^2\mathbf{r}_{iT} d^2\mathbf{p}_{iT}} \Big|_{|y_i| \leq \Delta y/2} \\ &\times \int \prod_{i=1}^3 d\eta_i dy_i \delta(\eta_i - y_i) F_B(x_1, x_2, x_3; p_1, p_2, p_3) \\ &\times \delta^{(2)}\left(\mathbf{p}_T - \sum_{i=1}^3 \mathbf{p}_{iT}\right). \end{aligned} \quad (18)$$

In the above, g_B is the statistical factor for formation of a baryon from three quarks. For baryons and antibaryons considered in present study, i.e., p , Δ , \bar{p} and $\bar{\Delta}$, the statistical factors are $g_p = g_{\bar{p}} = 1/108$ and $g_\Delta = g_{\bar{\Delta}} = 1/54$. The above formula can also be used for antibaryons by replacing quark momentum spectra by the momentum spectra of antiquarks.

III. PARTON DISTRIBUTIONS

We consider central Au+Au collisions (0 – 10%) at 200 AGeV, available at RHIC. In these collisions, hard processes between initial nucleons lead to production of minijets with large transverse momentum. Also, a quark-gluon plasma is expected to be formed from soft processes in the collisions. In this section, both parton momentum spectra in minijets and in the quark-gluon plasma are introduced.

A. minijet partons

Partons at high transverse momenta (usually greater than 2 GeV) are mainly from the minijets produced in initial hard collisions among nucleons. The transverse momentum distribution of minijet partons in the midrapidity can be obtained from an improved perturbative QCD calculation [13]. It is given by $dN_{\text{jet}}/d^2p_T = 1/\sigma_{\text{tot}}^{0-10} d\sigma_{\text{jet}}/d^2p_T$ in terms of $\sigma_{\text{tot}}^{0-10}$ corresponding to the total cross section at central 10% of the collisions and the jet production cross section from nucleus-nucleus collisions,

$$\begin{aligned} \frac{d\sigma_{\text{jet}}}{d^2\mathbf{p}_T} &= \int d^2\mathbf{b} d^2\mathbf{r} t_{\text{Au}}(\mathbf{r}) t_{\text{Au}}(\mathbf{b} - \mathbf{r}) \\ &\times \sum_{ab} \int dx_a dx_b d^2\mathbf{k}_{aT} d^2\mathbf{k}_{bT} g(\mathbf{k}_{aT}) g(\mathbf{k}_{bT}) \\ &\times f_{a/\text{Au}}(x_a, Q^2) f_{b/\text{Au}}(x_b, Q^2) \\ &\times \frac{\hat{s}}{\pi} \delta(\hat{s} + \hat{t} + \hat{u}) \frac{d\sigma^{ab}}{d\hat{t}}. \end{aligned} \quad (19)$$

In the above, $t_A(\mathbf{r})$ is the thickness function of Au at transverse radius \mathbf{r} given by integrating the nuclear density distribution along the longitudinal direction. The

parton distribution function in a nucleon in the nucleus Au is denoted by $f_{a/\text{Au}}(x, Q^2)$ including transverse smearing $g(\mathbf{k}_T)$. The cross section $d\sigma^{ab}/d\hat{t}$ is the parton scattering cross section. Kinematic details and a systematic analysis of pp collisions can be found in Ref. [13]. Using the GRV94 LO result for the PDF [14] and the KKP fragmentation function from Ref. [15], measured data in the reaction $pp \rightarrow \pi^0 X$ at $\sqrt{s} = 200$ GeV can be reproduced with $Q = 0.75p_T$ and $\langle k_T^2 \rangle = 2$ GeV².

In heavy ion collisions at RHIC, minijet partons are expected to lose energy by radiating soft partons as they traverse through the quark-gluon plasma. This effect can be taken into account by lowering their transverse momenta by the energy loss ΔE , which depends on both the parton energy E and an effective opacity parameter L/λ according to the GLV model [16].

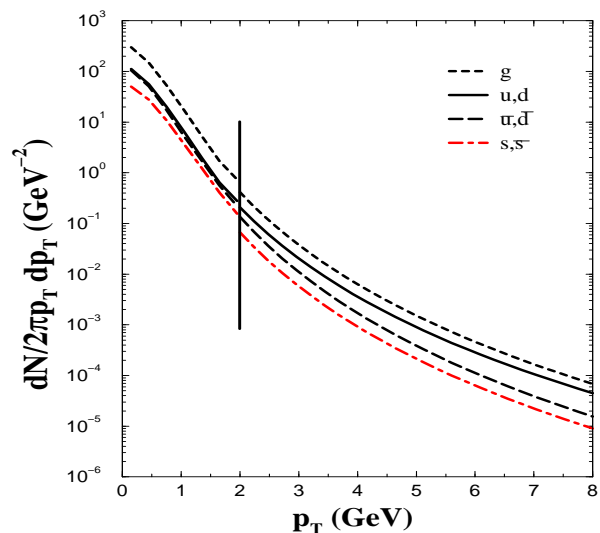


FIG. 1: Transverse momentum distributions of partons at hadronization in Au+Au collisions at $\sqrt{s} = 200$ AGeV for gluons (short-dashed curve), u and d (solid curve), \bar{u} and \bar{d} (dashed curve) as well as s and \bar{s} (dash-dotted curve) quarks. Minijet partons have transverse momenta greater than 2 GeV, while partons from the quark-gluon plasma have transverse momenta below 2 GeV.

Taking as momentum cutoff $p_0 = 2$ GeV/c for minijet partons and using an effective opacity $L/\lambda = 3.5$ as extracted from fitting the spectrum of high transverse momentum pions measured at RHIC [16, 17], the transverse momentum spectra of minijet partons at midrapidity ($y = 0$) in central Au+Au collisions at $\sqrt{s} = 200$ AGeV are shown in Fig. 1 for gluons (short-dashed curve), u and d (solid curve), \bar{u} and \bar{d} (dashed curve) as well as s and \bar{s} (dash-dotted curve) quarks. These spectra can be parametrized as

$$\frac{dN_{\text{jet}}}{d^2\mathbf{p}_T} = A \left(\frac{B}{B + p_T} \right)^n, \quad (20)$$

Values for the parameters A , B , and n for gluons, light and strange quarks and antiquarks are given in Table I.

For later calculation of parton coalescence probability, masses of minijet partons are taken to be the current quark masses, i.e., 10 MeV for light quarks and 175 MeV for strange quarks. Also, we assume that the rapidity distribution of minijet partons is uniform in the rapidity range of $y \in (-0.5, +0.5)$ considered in the present study.

TABLE I: Parameters for minijet parton distributions given in Eq.(20) at midrapidity from Au+Au at $\sqrt{s} = 200$ GeV.

	$A[1/\text{GeV}^2]$	$B[\text{GeV}]$	n
g	3.2×10^4	0.5	7.1
u,d	9.8×10^3	0.5	6.8
\bar{u}, \bar{d}	1.9×10^4	0.5	7.5
s, \bar{s}	6.5×10^3	0.5	7.4

B. the quark-gluon plasma

For partons in the quark-gluon plasma, their transverse momentum spectra are taken to have an exponential form. For their longitudinal momentum distribution, we assume that they are boost-invariant, i.e., they have a uniform rapidity distribution in the range $y \in (-0.5, +0.5)$. To take into account collective flow of quark-gluon plasma, these partons are boosted by a flow velocity $\mathbf{v}_T = \beta_0(\mathbf{r}_T/R_\perp)$, depending on their transverse radial positions r_T . Here, R_\perp is the transverse size of the quark-gluon plasma at hadronization, and β_0 is the collective flow velocity of the quark-gluon plasma and is taken to be $0.5c$. In this case, the light quarks and antiquarks transverse momentum spectra are given by

$$\frac{dN_{q,\bar{q}}}{d^2\mathbf{r}_T d^2\mathbf{p}_T} = \frac{g_{q,\bar{q}} \tau m_T}{(2\pi)^3} \times \exp\left(-\frac{\gamma_T(m_T - \mathbf{p}_T \cdot \mathbf{v}_T \mp \mu_q)}{T}\right), \quad (21)$$

where $g_q = g_{\bar{q}} = 6$ are the spin-color degeneracy of light quarks and antiquarks, and the minus and plus signs are for quarks and antiquarks, respectively. The slope parameter T is taken to be $T = 170$ MeV, consistent with the phase transition temperature ($T \sim 165 - 185$ MeV) from lattice QCD calculations. Masses of light quarks and antiquarks are taken to be $m_q = m_{\bar{q}} = 300$ MeV, similar to the masses of constituent quarks due to possible nonperturbative effects in the quark-gluon plasma near hadronization [18]. For the quark chemical potential μ_q , we use a value of $\mu_q = 10$ MeV to give a light antiquark to quark ratio of 0.89, which would then lead to an antiproton to proton ratio of about $(0.89)^3 = 0.7$, consistent with the observed ratio at midrapidity in heavy ion collisions at RHIC. The transverse flow effect is taken into account through the factor $\gamma_T = 1/\sqrt{1 - v_T^2}$.

The momentum spectra for strange quarks and antiquarks are similar to Eq.(21) with m_q replaced by the

strange quark mass $m_s = m_{\bar{s}} = 475$ MeV and μ_q replaced by $\mu_q - \mu_s$. The strange chemical potential μ_s is taken to have the same value as μ_q in order to have same strange and antistrange quarks numbers. The resulting strange quark to light quark ratio is then about 0.27. Including contribution from decays of ρ and K^* , this would then give a final $K^-/K^+ = 0.89$ and $K^-/\pi^- = 0.24$, comparable to experimental data at midrapidity from RHIC. Eq. (21) also applies to gluons after replacing g_q by the gluon spin-color degeneracy $g_g = 16$ and dropping the chemical potential. For the gluon mass, we take it to be similar to that of light quarks in order to take into account nonperturbative effects in the quark-gluon plasma.

Although the shape of quark-gluon plasma is nearly cylindrically symmetric, its parton momentum distribution is azimuthally asymmetric as shown by the finite elliptic flow of hadrons observed in experiments. Since we are interested in hadron spectra that are integrated over the azimuthal angle, including such asymmetry is not expected to change much our results. Nonetheless, the Monte-Carlo method to be described in Section IV to evaluate the coalescence formula can be easily extended to take into account such effects in order to study the relation between the elliptic flow of partons and those of hadrons as suggested in Ref. [2] and to be studied in Section VII.

The quark-gluon plasma is further assumed to have a transverse radius of $R_\perp = 8.3$ fm at proper time $\tau = 4$ fm, corresponding to a volume of $V = 900$ fm³. Positions of partons in the transverse direction are taken to have a uniform distribution. Their longitudinal positions are then determined by $z = \tau \sinh y$, as we have assumed that $\eta = y$ due to assumed Bjorken correlation. The resulting total transverse energy per unit rapidity from both the expanding quark-gluon plasma and minijet partons is about 590 GeV and is consistent with that measured by the PHENIX collaboration [19]. Most of this transverse energy comes from soft QGP partons as the contribution of minijet partons is only about 10%. The resulting parton density is about $\rho_{\text{parton}} \sim 1$ fm⁻³. The thermal parton spectra below the momentum cutoff $p_0 = 2$ GeV from the quark-gluon plasma including the collective flow effect are shown in Fig. 1 for gluons (short-dashed curve), u and d (solid curve), \bar{u} and \bar{d} (dashed curve) as well as s and \bar{s} (dash-dotted curve) quarks. Because of scattering of minijet partons with thermal partons as they traverse the quark-gluon plasma, those with momentum around p_0 are expected to be thermalized with partons in the quark-gluon plasma, leading to a smooth spectrum around p_0 . In the present study, we neglect this effect.

IV. THE MONTE-CARLO METHOD

In our previous study [5], only partons at midrapidity ($y = 0$) are considered. Furthermore, only comoving partons, i.e., partons with momenta in the same transverse direction are allowed to coalesce to hadrons. In

these limits, the coalescence formula is reduced to a one-dimensional integral for mesons and a two-dimensional integral for baryons. In the present study, we do not introduce these simplifications. Instead, the multi-dimensional integrals in the coalescence formula, given by Eqs.(12) and (18) are evaluated by the Monte-Carlo method via test particles. Specifically, we introduce a large number of test partons with uniform momentum distribution. To take into account the large difference between numbers of thermal and minijet partons, a test parton with momentum \mathbf{p}_T is given a probability that is proportional to the parton momentum distribution, e.g., $dN_q/d^2\mathbf{p}_T$ for quarks, with the proportional constant determined by requiring that the sum of all parton probabilities is equal to the parton number. With test partons, the coalescence formulas, Eqs.(12) and (18), are rewritten as

$$\frac{dN_M}{d^2\mathbf{p}_T} = g_M \sum_{i,j} P_q(i)P_{\bar{q}}(j)\delta^{(2)}(\mathbf{p}_T - \mathbf{p}_{iT} - \mathbf{p}_{jT}) \times f_M(x_i, x_j; p_i, p_j). \quad (22)$$

and

$$\frac{dN_B}{d^2\mathbf{p}_T} = g_B \sum_{i \neq j \neq k} P_q(i)P_q(j)P_q(k) \times \delta^{(2)}(\mathbf{p}_T - \mathbf{p}_{iT} - \mathbf{p}_{jT} - \mathbf{p}_{kT}) \times f_B(x_i, x_j, x_k; p_i, p_j, p_k). \quad (23)$$

In the above, $P_q(i)$ and $P_{\bar{q}}(j)$ are probabilities carried by i th test quark and j th test antiquark.

The Monte-Carlo method introduced here allows us to treat the coalescence of low momentum partons on the same footing as that of high momentum ones. We find that despite a decrease of eight orders-of-magnitude in real particle spectra, about equal numbers of test hadrons are formed at all momenta.

V. HADRON TRANSVERSE MOMENTUM SPECTRA

In this section, we show results for the transverse momentum spectra of pions, antiprotons, and antikaons using the model described in previous sections. For the coalescence contribution, we first take into account the effects due to gluons in the quark-gluon plasma and minijets by converting them to quarks and antiquark pairs with probabilities according to the flavor compositions in the quark-gluon plasma, as assumed in the ALCOR model [7]. For both mesons and baryons, we include not only coalescence of hard and soft partons as in Ref.[5] but also that among soft as well as hard partons. Furthermore, we include stable hadrons such as pion, nucleon (antinucleon), and kaon (antikaon) as well as unstable resonances such as ρ , Δ , and K^* . Since the coalescence model can be viewed as formation of bound states from interacting particles with energy mismatch

balanced by other particles in the system, neglecting such off-shell effects is reasonable if the energy mismatch is small. The model is thus applicable for rho and nucleon (antinucleon) production when we take into account quark masses. For other hadrons, the coalescence probability is expected to be reduced as a result of energy mismatch. The reduction factor can in principle be estimated by evaluating the transition probability in the presence of other particles. Since the coalescence radii Δ_x and Δ_p are treated as parameters in our study, the off-shell effects can be phenomenologically taken into account by using different coalescence radii for different hadrons. However, for simplicity we use same spatial coalescence radius $\Delta_x = 0.85$ fm and momentum coalescence radius $\Delta_p = 0.24$ for both mesons and baryons. We note that there are more ρ and K^* than pion and kaon produced from parton coalescence. The pion, proton, and kaon transverse momentum spectra from parton coalescence shown below include contributions from decays of rho, K^* , and Δ .

We have also included contributions to hadron production from minijet fragmentations. These are obtained using the KKP fragmentation function [15], which has been shown to reproduce measured high transverse momentum particles at RHIC. Explicitly, hadron momentum spectra are related to minijet parton momentum spectra by

$$\frac{dN}{d^2\mathbf{p}_{\text{had}}} = \sum_{\text{jet}} \int dz \frac{dN}{d^2\mathbf{p}_{\text{jet}}} \frac{D_{\text{had}/\text{jet}}(z, Q^2)}{z^2}, \quad (24)$$

where $z = p_{\text{jet}}/p_{\text{had}}$ is the fraction of minijet momentum carried by the formed hadron and $Q = p_{\text{had}}/2z$ is the momentum scale for the fragmentation process. The KKP fragmentation function is denoted by $D_{\text{had}/\text{jet}}(z, Q^2)$.

Before we show the results for hadron spectra and elliptic flows, we would like to point out that the coalescence model as formulated here is applicable if the number of hadrons produced is much less than the parton numbers. In this respect, results for hadrons with momenta above about 1 GeV/c, which account for about 5% of all partons, are reliable. For lower momentum hadrons, one needs to impose conservation of parton number in converting them to hadrons via coalescence. This correction has not been included in present study.

A. pion transverse momentum spectrum

In Fig. 2, we show the transverse momentum spectrum of pions formed directly from parton coalescence (dashed curve). Pions from fragmentations of minijet partons are shown by dash-dotted curve. It is seen that pions from parton coalescence dominate low transverse momenta while those from minijet fragmentations are important at high transverse momenta. The two contributions have a similar magnitude at transverse momentum of about 3 GeV. Also shown in the figure is the total pion transverse momentum spectrum from the two con-

tributions (solid curve). Compared with measured spectrum from the PHENIX Collaboration [20] (filled circles), the predicted spectrum of directly produced pion at low transverse momenta is much below experimental data.

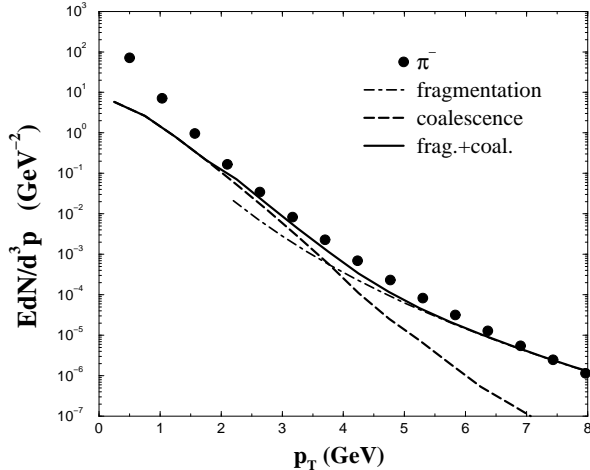


FIG. 2: Pion transverse momentum spectra from Au+Au collisions at $\sqrt{s} = 200$ AGeV: direct pion production from parton coalescence (dashed curve); pions from minijet fragmentations (dash-dotted curve); and sum from the above two contributions (solid curve). Parametrized experimental π^0 data [20] are shown by filled circles.

Since ρ , K^* , and Δ decay to pions, we have also included their contributions to the pion transverse momentum spectrum. It is found that rho meson decays contribute significantly to the pion spectrum at low transverse momenta and bring the final pion spectrum, shown by the solid curve in Fig. 3, in good agreement with experimental data. Also shown in this figure by the dashed curve is the pion spectrum without including contribution from coalescence of minijet partons with partons in the quark-gluon plasma. It underestimates the pion spectrum at intermediate transverse momenta around 3.5 GeV/c. The contribution from coalescence of partons from minijets with those from the quark-gluon plasma is more clearly seen from the ratio of pion spectra with and without this contribution, shown in the inset of Fig. 3, which is more than a factor of 2 at transverse momenta around 4 GeV/c. Our results thus confirm our previous results in Ref.[5] based on a parametrized pion spectrum from hadronization of the quark-gluon plasma.

B. antiproton transverse momentum spectrum

In Fig. 4, we show the antiproton spectrum including those from decays of $\bar{\Delta}$ for Au+Au collisions at $\sqrt{s} = 200$ AGeV. Results for both with (solid curve) and without (dashed curve) contributions from coalescence of minijet partons with partons from the quark-gluon plasma are shown. They include contributions from fragmentations of minijet partons (dash-dotted curve). The contribution from coalescence of soft and hard partons becomes

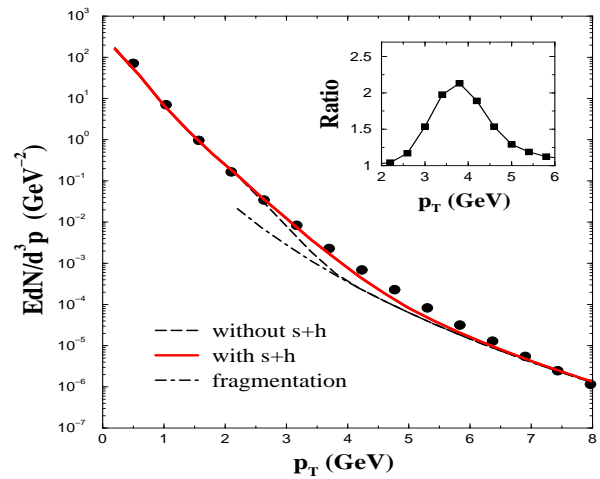


FIG. 3: Pion transverse momentum spectra from Au+Au collisions at $\sqrt{s} = 200$ AGeV with (solid curve) and without (dashed curve) contributions from coalescence of minijet partons with the quark-gluon partons. Parametrized experimental π^0 data [20] are shown by filled circles. Ratio of the two spectra is given in the inset.

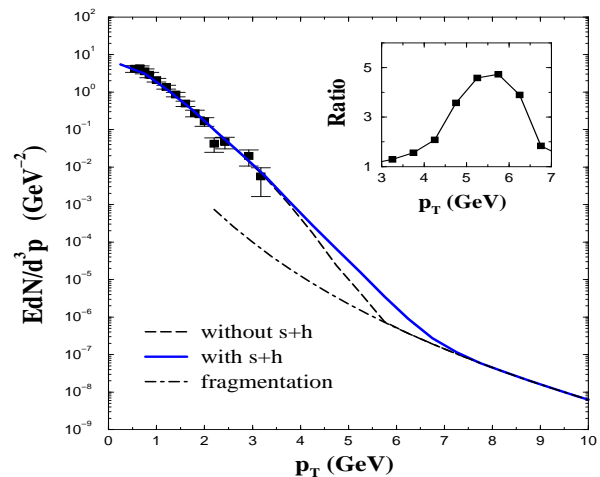


FIG. 4: Transverse momentum spectra of antiprotons from Au+Au collisions $\sqrt{s} = 200$ AGeV. The dashed curve includes hadrons only from coalescence of partons in the quark-gluon plasma and from independent fragmentations of minijet partons (dash-dotted curve). Adding also hadrons from coalescence of minijet partons with partons in the quark-gluon plasma gives the solid curve. Ratio of the solid to the dashed curve is given in the inset. Experimental p^- data [21] at 130 AGeV are shown by filled circles.

important when the transverse momentum is above 3 GeV/c, which is somewhat higher than in the case of pion transverse momentum spectrum. Since there are no published experimental data for antiproton transverse momentum spectrum from Au+Au collisions at 200 AGeV, we compare our predictions with the experimental data from the PHENIX collaboration for Au+Au collisions at $\sqrt{s} = 130$ AGeV [21], shown by filled squares for transverse momenta below 3 GeV/c. Both predictions with

and without contributions from coalescence of minijet partons with partons from the quark-gluon plasma are comparable to the experimental data. Shown in the inset of this figure is their ratio as a function of transverse momentum. It is seen that the ratio is close to a factor of 5 at transverse momenta around 5.5 GeV/c. The contribution from coalescence of minijet partons with those from the quark-gluon plasma is thus more important for antiprotons than for pions. It would be of great interest to have experimental data for antiprotons at such high transverse momenta to verify our predictions.

C. antiproton to pion ratio

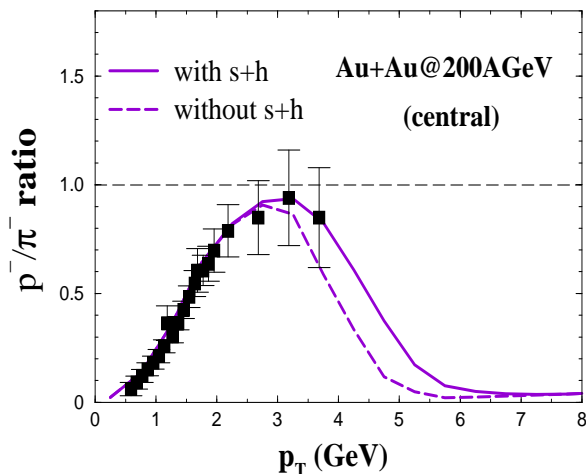


FIG. 5: Antiproton to pion ratio from Au+Au collisions at $\sqrt{s} = 200$ AGeV. Solid and dashed curves are, respectively, results with and without contributions to antiprotons from coalescence of minijet partons with those from the quark-gluon plasma. Filled squares are the experimental data [11].

The antiproton to pion ratio is shown in Fig. 5 as a function of transverse momentum. The solid curve is the result including contributions from both parton coalescence and minijet fragmentations. The ratio increases with transverse momentum up to about 3 GeV/c and decreases with further increasing transverse momentum as in the experimental data [11] shown by filled squares. At high transverse momenta, the antiproton to pion ratio becomes very small as it is largely determined by the results from pQCD [22]. Neglecting the contribution to antiproton production from coalescence of minijet partons with partons from the quark-gluon plasma reduces the antiproton to pion ratio at transverse momenta above 2.5 GeV as shown by the dashed curve in Fig. 5.

The enhanced antiproton to pion ratio at intermediate transverse momenta was previously attributed to antiproton production from the baryon junctions in incident nucleons [23]. The possibility of enhanced baryon to pion ratio due to parton coalescence was suggested in Ref. [2]. Using a parton distribution function that is

fitted to measured pion transverse momentum spectrum, a parton recombination model similar to the coalescence model indeed leads to a large antiproton to pion ratio at intermediate transverse momenta [3]. In Ref. [4], the antiproton to pion anomaly is explained by the recombination of partons from a quark-gluon plasma with a high effective temperature. Our model further introduces coalescence of minijet partons with partons in the quark-gluon plasma. This makes it possible to account for both the large antiproton to pion ratio at intermediate transverse momenta and its behavior at low transverse momenta.

In our previous work [5], an increasing antiproton to pion ratio at low transverse momenta was also seen, but it was obtained by using different inverse slope parameters for antiproton and pion transverse momentum spectra. In contrast, results obtained in the present work are due to coalescence of soft partons from the quark-gluon plasma.

D. kaon transverse momentum spectrum and kaon to pion ratio

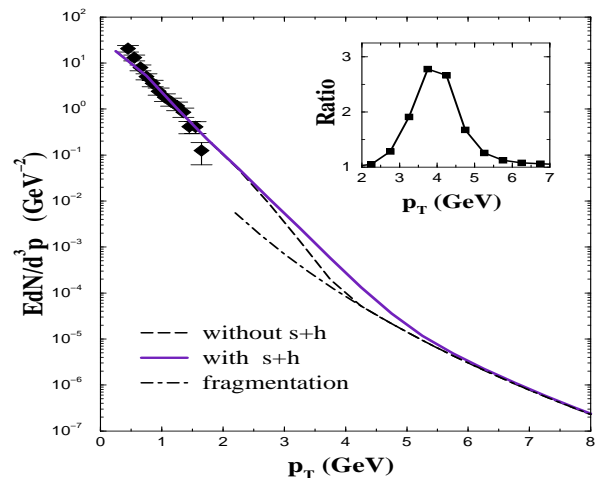


FIG. 6: Transverse momentum spectra of K^- from Au+Au collisions at $\sqrt{s} = 200$ AGeV. The dashed curve includes contributions only from coalescence of partons in the quark-gluon plasma and hadrons from independent fragmentations of minijet partons (dash-dotted curve). Adding also hadrons from coalescence of minijet partons with partons in the quark-gluon plasma gives the solid curve. Ratio of the solid to the dashed curve is given in the inset. Experimental K^- data [21] at 130 AGeV are shown by filled circles.

In Fig. 6, we show the antikaon spectrum including those from decays of K^{*-} for Au+Au collisions at $\sqrt{s} = 200$ AGeV. Results including antikaon production from coalescence of soft partons from the quark-gluon plasma are shown by dashed curve while those including also coalescence between minijet partons with the quark-gluon plasmas are shown by the solid curve. Contributions from minijet fragmentations (dash-dotted curve)

are also included. As for antiprotons, we compare these predictions with the experimental data shown by filled squares from the PHENIX collaboration for Au+Au collisions at $\sqrt{s} = 130$ AGeV [21], as there are no published data at $\sqrt{s} = 200$ AGeV. For the limited data below 2 GeV/c, the coalescence model reproduces them very well without the contribution from coalescence of minijet partons with partons from the quark-gluon plasma as the latter becomes important when the transverse momentum is above 2.5 GeV/c. Shown in the inset of Fig. 6 is the ratio of the predictions with and without the contribution from soft and hard parton coalescence as a function of transverse momentum. The ratio reaches a factor of close to 3 at transverse momentum around 4 GeV/c. The contribution to antikaons from coalescence of minijet partons with those from the quark-gluon plasma is thus comparable to that for pions.

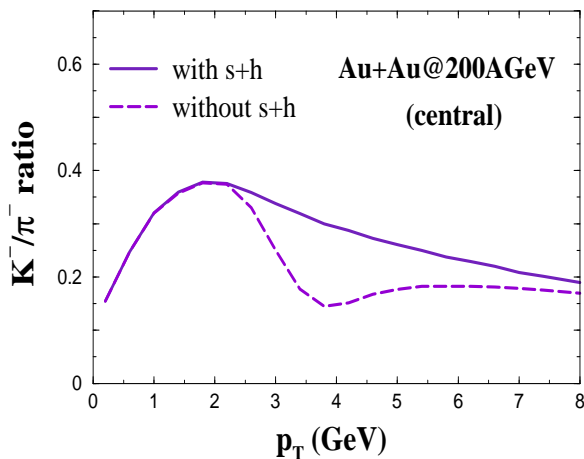


FIG. 7: Antikaon to pion ratio from Au+Au collisions at $\sqrt{s} = 200$ AGeV. Solid and dashed curves are, respectively, results with and without contributions to antikaon production from coalescence of minijet partons with those from the quark-gluon plasma.

The antikaon to pion ratio is shown in Fig. 7 as a function of transverse momentum. The solid curve is the result including contributions from both parton coalescence and minijet fragmentations. For transverse momenta below about 2 GeV/c, this ratio is similar to the antiproton to pion ratio except that its value is smaller. At higher transverse momenta, the antikaon to pion ratio decreases slightly and reaches the value predicted by pQCD at high transverse momenta [24], which gives a larger antikaon to pion ratio than the antiproton to pion ratio. Results without contribution to antikaon production from coalescence of minijet partons with partons from the quark-gluon plasma are given by the dashed curve, and it gives a smaller antikaon to pion ratio at intermediate transverse momenta compared to that with this contribution. Our results thus demonstrate again the importance of antikaon production from coalescence of partons from minijets and quark-gluon plasma.

VI. TRANSVERSE FLOW EFFECT

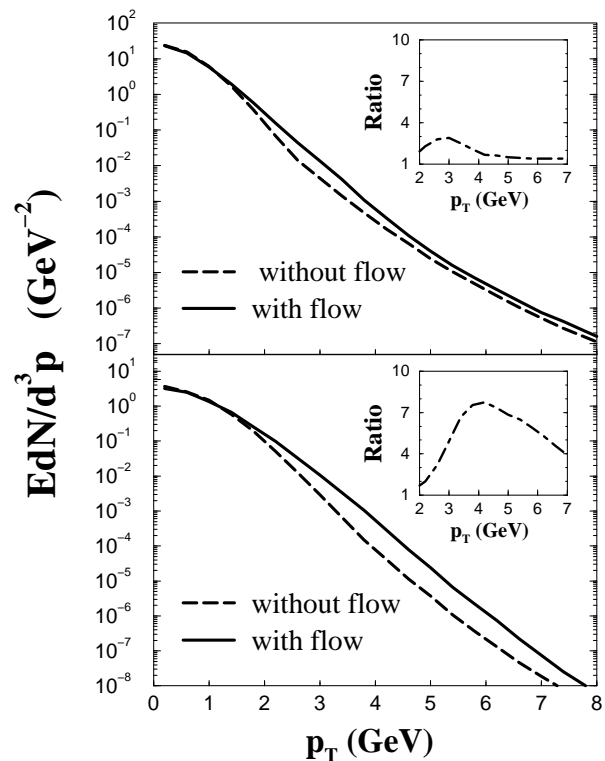


FIG. 8: Pion (upper panel) and antiproton (lower panel) transverse momentum spectra from coalescence of partons in the quark-gluon plasma with (solid curves) and without (dashed curves) collective transverse flow in the quark-gluon plasma. Ratio of these two results are shown in the insets.

It is interesting to study the effect of transverse flow of quark-gluon plasma on the transverse momentum spectra of produced hadrons. In fact, the increase of antiproton to pion ratio at low transverse momenta was believed to be due to a stronger transverse flow effect on protons than on pions [25]. Such effect was assumed in our previous study [5] by using a larger inverse slope parameter for the antiproton transverse momentum spectrum than that for pions. In the present model, soft hadrons are produced from coalescence of partons in the quark-gluon plasma, which is given a collective flow velocity of $0.5c$, and the resulting antiproton to pion ratio at low transverse momentum is found to increase with transverse momentum. To see if this is due to the collective flow effect introduced in the model, we have repeated the calculations without transverse flow effect on antiprotons. These results, which include only contribution to antiproton production from coalescence of partons in the quark-gluon plasma, are shown in Fig. 8 by dashed curves for pions (upper panel) and antiprotons (lower panel). Compared with results with a collective flow velocity of $0.5c$, shown by solid curves in Fig. 8, collective flow affects the pion and antiproton spectra mainly at transverse momenta above 1.5 GeV/c, and its effect is stronger for antipro-

tons than for pions. The reason that for low transverse momenta the inverse slope parameter for pions remains smaller than that for antiprotons in the absence of collective flow is due to the fact that most low transverse momentum pions are from decays of rho mesons, which gives a smaller effective slope parameter for pions than that of directly produced pions. Our results thus demonstrate that the increase seen in the antiproton to pion ratio at low transverse momenta is not necessarily due to the collective flow of quark-gluon plasma.

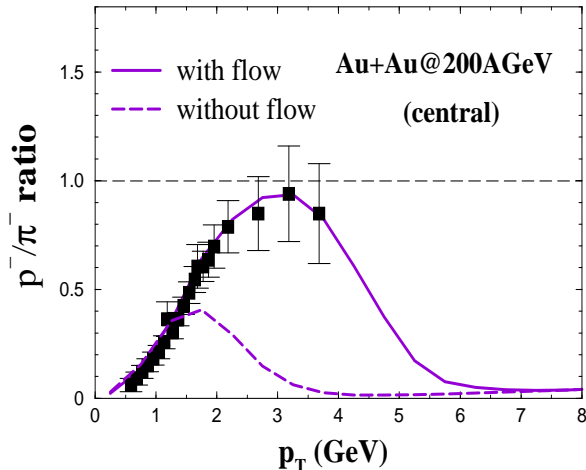


FIG. 9: Antiproton to pion ratio with (solid curve) and without (dashed curve) collective flow in the quark-gluon plasma. Experimental data are shown by filled squares.

Since collective flow affects hadron spectra at intermediate transverse momenta as shown in Fig.8 and its insets, where the ratio of pion or antiproton spectrum obtained with and without collective flow in the quark-gluon plasma is shown, it is expected to have a large effect on the antiproton to pion ratio at these momenta. This is shown in Fig.9, where the antiproton to pion ratio is given for both with (solid curve) and without (dashed curve) collective flow effect on protons. It is seen that collective flow enhances significantly this ratio for transverse momenta between 2 and 5 GeV/c. The collective flow effect on intermediate transverse momentum antiprotons is thus as strong as the effect due to coalescence of partons from minijets with those from the quark-gluon plasma, shown in Fig. 5. To confirm the mechanism for antiproton production from coalescence of minijet and quark-gluon plasma partons, it is thus important to have a quantitative understanding of collective flow in the quark-gluon plasma.

VII. ELLIPTIC FLOWS

The parton coalescence model based on the test particle Monte-Carlo method is also useful for studying other observables at RHIC. One problem that can be addressed with this model is to study how elliptic flows of hadrons

are related to that of partons [26, 27]. We carry out such a study following the idea of Ref. [3], where the parton transverse momentum distribution is extracted from fitting the pion transverse momentum spectrum using the quark recombination or coalescence model and is then used to predict that of antiprotons. Here, we extract the elliptic flows of light and strange quarks by fitting the measured pion and kaon elliptic flows based on the coalescence model. The resulting quark elliptic flows are then used to predict the elliptic flows of protons, Λ , Ω , and phi mesons.

The elliptic flow is a measure of the anisotropy of particle transverse momentum spectrum, i.e.,

$$v_2 = \left\langle \frac{p_x^2 - p_y^2}{p_x^2 + p_y^2} \right\rangle, \quad (25)$$

where the transverse axes x and y are, respectively, in and out of the reaction plane. Including transverse momentum anisotropy, the quark transverse momentum distribution is given by

$$\frac{dN_q}{d^2\mathbf{p}_T} = \frac{dN_q}{p_T dp_T d\phi} = \frac{dN_q}{p_T dp_T} [1 + v_2 \cos(2\phi)], \quad (26)$$

where ϕ is the azimuthal angle in the transverse plane.

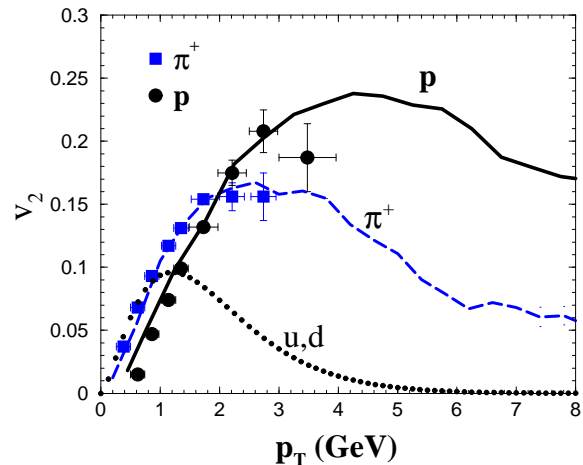


FIG. 10: Elliptic flows of pions (dashed curve) and protons (solid curve) as functions of transverse momentum. Elliptic flow of light quarks and antiquarks is given by dotted curve. Experimental data [28] are shown by filled squares for pions and filled circles for protons.

In Fig. 10, we show by dotted curve the elliptic flows of light quarks and antiquarks together with the pion elliptic flow shown by dashed curve, which is supposed to reproduce the measured pion elliptic flow given by filled squares [28]. The predicted proton elliptic flow obtained from the quark and antiquark elliptic flows is then given by the dashed curve and is seen to agree with that measured in experiments shown by filled circles [28].

The elliptic flow of strange hadrons are shown in Fig. 11. The strange quark and antiquark elliptic flow (dotted curve) used to fit the measured kaon elliptic flow

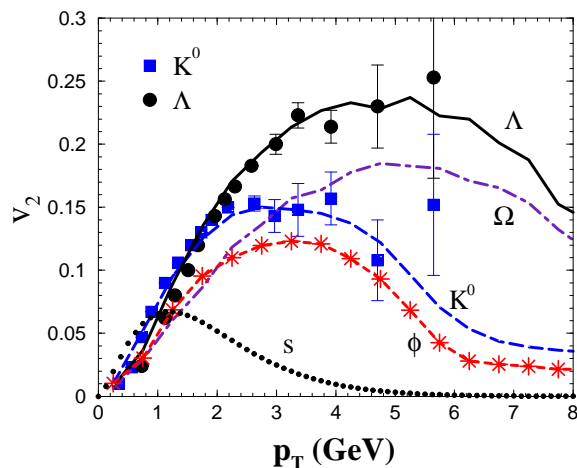


FIG. 11: Elliptic flows of kaons (solid curve), phi mesons (dashed curve with stars), Λ (dashed curve), and Ω (dash-dotted curve). Elliptic flow of strange quarks and antiquarks is given by dotted curve. Experimental data [29] are shown by filled squares for kaons and circles for Λ .

[29] shown by filled squares for data and dashed curve from the coalescence model. The predicted Λ elliptic flow shown by dashed curve is seen to agree with the available experimental data [29] given by filled circles. We have also predicted the phi meson (dashed curve with stars) and Ω elliptic flows (dash-dotted curve), which are smaller than the kaon and Λ elliptic flow, respectively, as a result of smaller (about 30%) strange quark elliptic flows than that of light quarks.

For all hadron considered here, decrease of their elliptic flows at high transverse momenta is due to our assumption that high transverse momentum minijet partons and hadrons from minijet fragmentations have vanishing elliptic flows. Of course, if high transverse momentum minijet partons also develop elliptic flow as suggested in Ref. [30], our results on hadron elliptic flows at high transverse momenta should be modified.

VIII. SUMMARY AND OUTLOOK

In this paper, we have studied the hadronization of quark-gluon plasma and minijet partons produced in relativistic heavy ion collisions in terms of the parton coalescence model. The momentum spectra of partons in the quark-gluon plasma is taken to have an exponential form with inverse slope parameter similar to the phase transition temperature, while partons in the minijets have power-law spectra. The flavor compositions in the quark-gluon plasma is determined by the experimentally measured antiproton to proton ratio and strange to nonstrange particle ratios. The volume of quark-gluon plasma is then fixed by the total transverse energy measured in experiments. A collective flow is introduced in the quark-gluon plasma with a flow velocity comparable to that extracted from experiments. To take into account

the vast difference in the magnitude of the minijet parton transverse momentum spectrum and that of partons in the quark-gluon plasma, a test particle Monte-Carlo method has been introduced to efficiently evaluate the coalescence probability of partons. Both soft partons from the quark-gluon plasma and hard partons from minijets are used in the coalescence model to produce hadrons such as pions, kaons (antikaons), rho mesons, K^* 's, nucleons (antinucleons), and Δ ($\bar{\Delta}$) resonances. Specifically, we have included coalescence of hard minijet partons with soft partons besides that among soft and hard partons.

The resulting pion, antikaon, and antiproton spectra are seen to agree with available experimental data from RHIC. For pions, contributions from rho decays are important in explaining the measured transverse momentum spectrum below 2 GeV/c. For intermediate transverse momentum spectra between 2 and 5 GeV/c, including contributions from coalescence of minijet partons with those from the quark-gluon plasma are important, leading to a factor of more than two enhancement compared to results without this contribution. We have also compared the transverse momentum dependence of antiproton to pion ratio to the experimental data. Results from the coalescence model are found to agree quite well with the available data, i.e., it increases with transverse momentum and reaches a value of about one at transverse momentum of about 3 GeV/c. With further increase in transverse momentum, our model predicts that the antiproton to pion ratio should decrease and approach the small value given by the pQCD. We have also calculated the antikaon to pion ratio as a function of transverse momentum. The result is similar to that for antiproton to pion ratio but with a smaller magnitude and a larger value at high transverse momenta. We further find that these ratios are reduced if antiproton production from coalescence of minijet partons with partons in the quark-gluon plasma is neglected. This effect is, however, comparable to that due to collective flow of quark-gluon plasma. To confirm the mechanism for antiproton production from coalescence of minijet partons with partons in the quark-gluon plasma thus requires a quantitative understanding of collective flow effects in the quark-gluon plasma.

We have also studied elliptic flows of hadrons using quark and antiquark elliptic flows fitted to the measured pion and kaon elliptic flows. Predicted proton and Λ elliptic flows agree with those measured in experiments. We have further predicted the Ω elliptic flow, which is smaller than other hadrons due to smaller strange quark elliptic flow than that of light quarks.

The parton coalescence model based on the test particle Monte-Carlo method can be further extended to include collision dynamics of partons and hadrons using parton and hadron transport models. This would make it possible to study effects due to final-state hadronic scattering on the transverse momentum spectra and elliptic flows of hadrons, which have been neglected in

present study as we have compared hadron spectra elliptic flows from parton coalescence directly with experimental data. Also, including parton scatterings would allow us to treat properly the parton spectrum around the cutoff momentum p_0 , resulting in a smooth spectrum at this momentum. It further makes it possible to determine both transverse and elliptic flows of partons from the collision dynamics instead of treating them as input as in the present study. Moreover, including expansion dynamics of the system will ensure that the total entropy does not decrease even though the entropy density is reduced when hadrons are formed from coalescence of partons.

Acknowledgments

This paper is based on work supported by the U.S. National Science Foundation under Grant No. PHY-0098805 and the Welch Foundation under Grant No. A-1358. V.G. is also supported by the National Institute of Nuclear Physics (INFN) in Italy, while P.L. by the Hungarian OTKA Grant Nos. T034269 and T043455. P.L. further thanks G. Papp and G. Fai for discussions on pQCD results.

-
- [1] Z. Lin and C.M. Ko, Phys. Rev. C **65**, 034904 (2002); Z. Lin, C.M. Ko, and S. Pal, Phys. Rev. Lett. **89**, 152301 (2002).
- [2] S.A. Voloshin, nucl-ex/0210014.
- [3] R.C. Hwa and C.B. Yang, Phys. Rev. C **67**, 034902 (2003); nucl-th/0301004; nucl-th/0302006.
- [4] R.J. Fries, B. Meuller, and C. Nonaka, S. Bass, nucl-th/0301087.
- [5] V. Greco, C.M. Ko, P. Lévai, Phys. Rev. Lett., in press; nucl-th/0301093.
- [6] Z. Lin and C.M. Ko, Phys. Rev. Lett. **89**, 202302 (2002).
- [7] T.S. Biró, P. Lévai, and J. Zimányi, Phys. Lett. B **347**, 6 (1995); Phys. Rev. C **59**, 1574 (1999); T.S. Biró, T. Csörgö, P. Lévai, and J. Zimányi, *ibid.* B **472**, 243 (2000).
- [8] P. Csizmadia and P. Lévai, Phys. Rev. C **61**, 031903 (2000); J. Phys. G **28**, 1997 (2002).
- [9] B. Zhang, C.M. Ko, B.A. Li, and Z. Lin, Phys. Rev. C **61**, 067901 (2000); *ibid.* **62**, 054905 (2000); **65**, 054909 (2002); Z. Lin, S. Pal, C.M. Ko, B.A. Li, and B. Zhang, *ibid.* **64**, 011902 (2001); Nucl. Phys. **A498**, 375c (2002).
- [10] X.N. Wang, Phys. Rev. C **58**, 2321 (1998).
- [11] K. Adcox, Phys. Rev. Lett. **88**, 242301 (2002); T. Chujo, nucl-ex/0209027; T. Sakaguchi, nucl-ex/0209030.
- [12] C. Dover, U. Heinz, E. Schnedermann, and J. Zimányi, Phys. Rev. C **44**, 1636 (1991).
- [13] Y. Zhang *et al.*, Phys. Rev. C **65**, 034903 (2002).
- [14] M. Glück, E. Reya, and A. Vogt, Z. Phys. C **67**, 433 (1995).
- [15] B.A. Kniehl, G. Kramer, and B. Pötter, Nucl. Phys. **B582**, 514 (2000); **B597**, 337 (2001).
- [16] P. Lévai *et al.*, Nucl. Phys. **A698**, 631 (2002); M. Gyulassy, P. Lévai, and I. Vitev, Phys. Lett. B **538**, 282 (2002).
- [17] M. Gyulassy, P. Lévai, and I. Vitev, Phys. Rev. Lett. **85**, 5535 (2000); Nucl. Phys. **B571**, 197 (2000); *ibid.* **B594**, 371 (2001); M. Gyulassy, I. Vitev, and X. N. Wang, Phys. Rev. Lett. **86**, 2537 (2001).
- [18] P. Lévai and U. Heinz, Phys. Rev. C **57**, 1879 (1998).
- [19] K. Adcox *et al.* (PHENIX Collaboration), Phys. Rev. Lett. **87**, 052301 (2001).
- [20] D. d'Enterria for the PHENIX Collaboration, hep-ex/0209051.
- [21] K. Adcox *et al.* (PHENIX Collaboration), Phys. Rev. Lett. **88**, 022301 (2002).
- [22] X. Zhang, G. Fai, and P. Lévai, Phys. Rev. Lett. **89**, 272301 (2002).
- [23] I. Vitev and M. Gyulassy, Phys. Rev. C **65**, 041902 (2002).
- [24] P. Lévai, G. Papp, G. Fai, and M. Gyulassy, nucl-th/0012017, LBNL-47163.
- [25] U. Heinz, talk presented at PANIC02, nucl-th/0212004.
- [26] D. Molnar and S. A. Voloshin, nucl-th/0302014.
- [27] Z. W. Lin and D. Molnar, nucl-th/0304045.
- [28] S. Esumi (PHENIX Collaboration), Proceedings of the 16th International Conference on Ultrarelativistic Nucleus-Nucleus Collisions, Nantes, France, July 18-24, 2002, nucl-exp/0210012.
- [29] R. Snellings (STAR Collaboration), 19th Winter Workshop on Nuclear Dynamics, nucl-ex/0305001.
- [30] M. Gyulassy, I. Vitev, X.N. Wang, and P. Huovinen, Phys. Rev. Lett. **86**, 2537 (2001); Phys. Lett. B **526**, 301 (2002).